# Sub-THz Electron Spin Resonance spectroscopy based on a Martin-Puplett interferometer

Christian Caspers,[1,*] Pedro Freire da Silva,[2] Murari Soundararajan,[1] M. Ali Haider,[3] and Jean-Philippe Ansermet[1]

[1] *Laboratoire de Physique des Matériaux Nanostructurés LPMN, École Polytechnique Fédérale de Lausanne EPFL, 1015 Lausanne, Switzerland*

[2] *Instituto Superior Técnico, Technical University of Lisboa, 49-001 Lisboa, Portugal*

[3] *Department of Chemical Engineering, Indian Institute of Technology Delhi, New Delhi 110016, India*

(Dated: January 13, 2016)

A 260-GHz electron spin resonance (ESR) spectrometer was developed using Martin-Puplett interferometry, quasi-optical isolation, beam focusing and electronic polarization control. Computer-aided design and polarization pathway simulation lead to the design of a mobile and compact system, featuring lateral dimensions less than a foot and high mechanical stability, with all components rated for power levels of several Watts. Benchmark results were obtained with ESR standards (BDPA, DPPH) using field modulation. Original high-field ESR of $4f$ electrons in $Sm^{3+}$-doped Ceria was detected using frequency modulation. For the narrow line of BDPA, our quasioptically focusing sample holder with distinct combinations of field and modulation frequency reaches a signal-to-noise ratio of 35 dB, corresponding to a detection limit of about $10^{14}$ spins.

## INTRODUCTION

Improving Electron Spin Resonance (ESR)[1] spectroscopy in order to explore for example the spin properties of novel oxide interfaces,[2–7] or of spin functional surfaces,[8–16] or to unravel details of the reactions taking place at the surface of catalysts[17–27] requires ever greater resolution and sensitivity. This implies the use of ever great applied fields, which require in turn sample irradiation frequencies in the sub-THz range.

While at frequencies of 150 GHz very sophisticated waveguides and cavities can still be designed,[28] the question remains at how to achieve proper excitation at frequencies beyond the highest r.f. frequencies (so-called $D$ band). Lynch *et al.* [29] showed that sub-THz radiation — a drastic shift from the conventional r.f. technology to free space quasioptical treatment — could be used for high-field ESR ($B_0 = 9\,\mathrm{T}$, $f_{h\nu} = 250\,\mathrm{GHz}$) with *quasioptical technology*.[29–33]

In their analysis of sub-THz continuous wave (cw) ESR spectrometers[34, 35] which operated quasioptically and in reflection mode, Earle *et al.* [34] estimated for the high-field ESR sensitivity in terms of the minimum number of spins $N_{\mathrm{min}}^{\mathrm{spins}}$ that can be detected,

$$N_{\mathrm{min}}^{\mathrm{spins}} \propto \frac{V_s T_s}{Q_L P_{h\nu}^{1/2}} \left( \frac{\Delta\omega_{pp}}{\omega_{h\nu}} \right) \qquad (1)$$

where $V_s$ and $T_s$ are sample volume and temperature, $Q_L$ the loaded quality factor, $P_{h\nu}$ and $\omega_{h\nu}$ denote the sub-THz irradiation power and frequency, and $\Delta\omega_{pp} = \gamma\,\Delta B_{pp}$ the peak width. While the sample itself, the quality factor and the temperature can easily be varied, the major challenge is to implement higher sub-THz irradiation frequency $\omega_{h\nu}$ and power $P_{h\nu}$.

Significant developments of high-field quasioptical ESR are ongoing,[32, 33, 36–40] where cw ESR has evolved up to $f_{h\nu} = 750\,\mathrm{GHz}$[41] and free electron lasers (FEL) can provide highest irradiation power (several kW) in pulsed or quasi-cw high-field ESR.[42–45] However, these spectrometers are highly specialized and operate in one dedicated high-field environment,[41] and a very recent commercial system provides a high ESR sensitivity but narrow (0.2 T) field sweep range.[46] A *compact and mobile quasioptical* ESR spectrometer is desirable, which combines sub-THz frequency acceptance of *very broad range* and operates with *different radiation sources* and laboratory cryostats containing samples conditioned according to specific research requirements. Recently, Armstrong *et al.* [47] have addressed this challenge, proposing a Martin-Puplett (MP) interferometer[48] on a compact quasioptical bridge with sub-THz (200 GHz) input and analysis of the signal reflected from the paramagnetic sample. Using quasioptics for the lower $G$ band (110–200 GHz), however, necessarily involves diffraction effects and standing waves in compact optical bridges, as the wavelength ($\sim 2\,\mathrm{mm}$) is one tenth of typical optical aperture sizes.

Here, we give details about the design and demonstrate the operation of a very compact quasioptical MP spectrometer for high-field ESR which works as a mobile platform on top of a high-field 9.4 T cryostat and admits user-selectable sub-THz sources. As we are using the *high-frequency end* of the $G$ band as irradiation for $B_1$ excitation, namely 245–285 GHz ($\lambda \leqslant 1.1\,\mathrm{mm}$), the advantages of optical focusing, lossless freespace transmission and diminished diffraction are feasible with a compact design — in contrast to bulky setups necessary for larger wavelength $W$ band or even 150 GHz specrometers. Our system features the use of standardized holders,[49] and operation on a superconducting magnet or as a table-top device, which is particularly useful during the adjustment and characterization of the polarization changing components. Challenges of standing waves and background

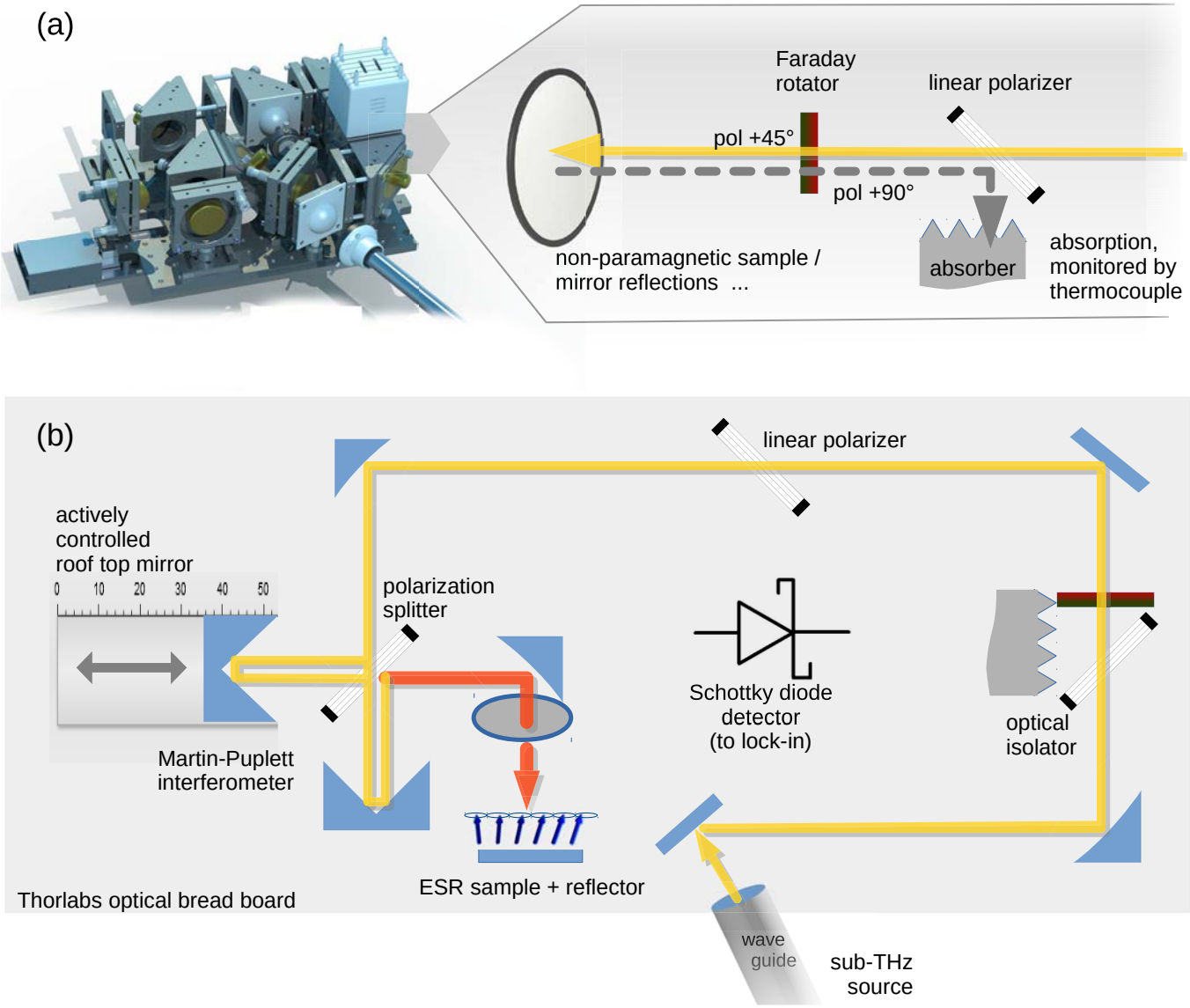


FIG. 1. Excitation pathway in the quasioptical MP spectrometer. (a) Metallic reflections (e.g. standing wave modes between surfaces, dashed grey) are deflected into an absorber by using the quasioptical isolation for 260 GHz. (b) Free space transmission (yellow) from the waveguide (sub-THz sources) along Au-coated elliptical mirros, linear polarizers, and the MP interferometer. The ESR sample with reflection mirror is located below a vertical corrugated waveguide inside an Oxford high-field magnet with continuous He flow cryostat (orange beam).

rejection were solved by the use of optical isolation[50] and MP interferometry,[47, 51] respectively.

We demonstrate the capabilities of the spectrometer with three experiments. First, the standard radical 2,2-diphenyl-1-picrylhydrazyl (DPPH) illustrates the gain in spectral resolution by direct comparison of $X$-band ESR with high-field 260 GHz ESR. Next, we present high-field ESR of doped Ceria powder, a material considered for catalysis ($CO_2$ reduction) and for solid oxide fuel cells (ionic conductivity). Here, Samarium sites in the $CeO_2$ lattice provide unpaired $4f$ spins. We distinguish $4f$ spins with different angular momenta in the very broad band spectral range 245–280 GHz using frequency modulation of the sub-THz irradiation. Third, we demonstrate with 1,3-bisdiphenylene-2-phenylallyl (BDPA), a radical that has a narrow ESR line, that the proper combination of an optically focusing sample holder with field modulation at high frequencies provides a distinct optimum in signal-to-noise ratio (SNR).

## QUASIOPTICAL 260 GHZ MP SPECTROMETER

In order to take advantage of the enhanced resolution and sensitivty of high-field ESR at 260 GHz, the MP spectrometer has to transmit the $B_1$ field and detect the

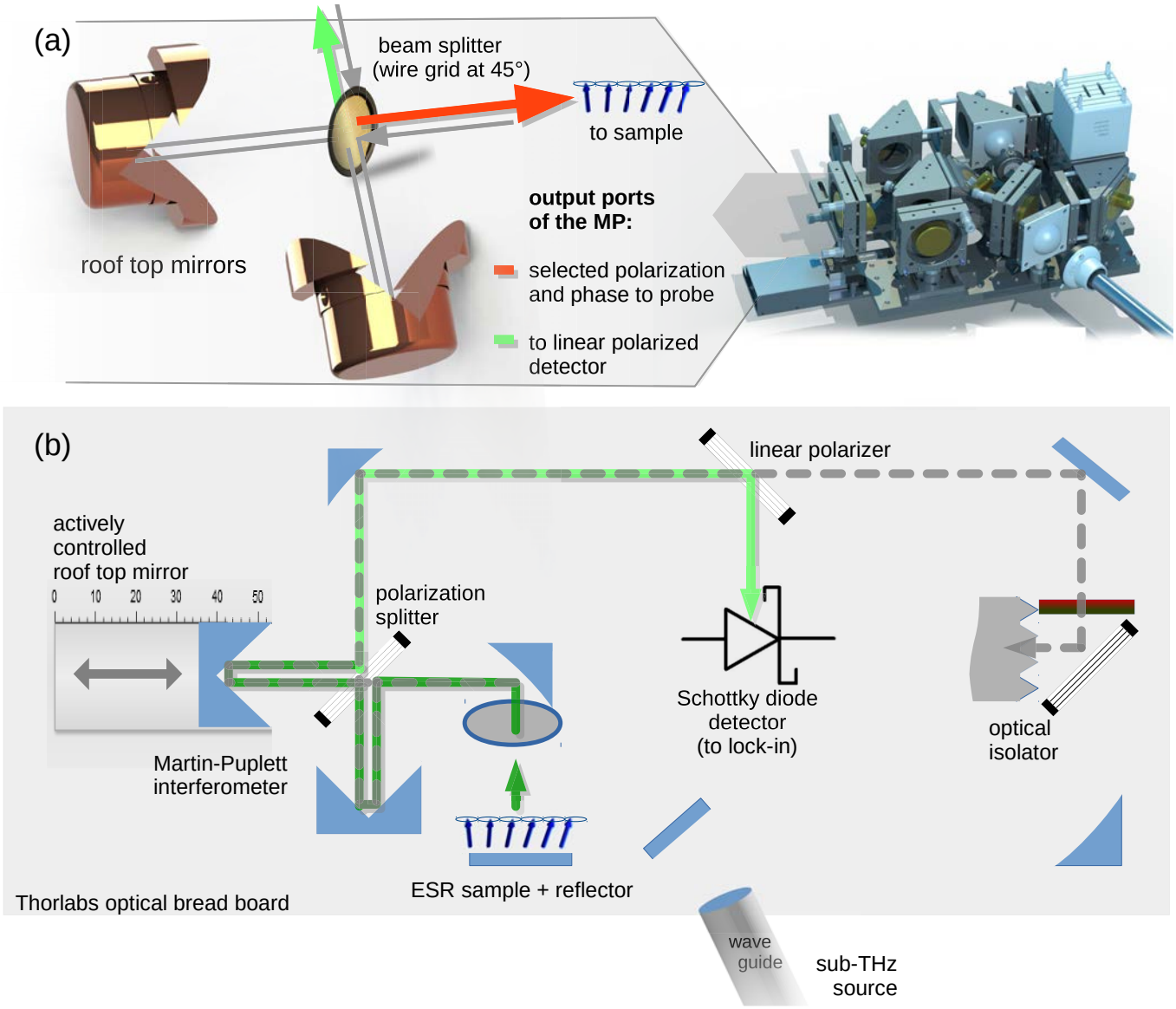


FIG. 2. Received beam pathway in the quasioptical MP spectrometer. (a) Roof top mirrors control the phase of orthogonal polarizations in the MP interferometer, thereby determine the sample excitation (light red) and fine tune the detectable polarization changes (light green). (b) The reflected and MP tuned signal is focused along elliptical mirrors and deflected by a grid into the sub-THz Schottky diode detector. Metallic reflections without polarization change are passed to the absorber.

returning $E$ field both with with minimal loss: a quasioptical pathway design is needed. Hereby, the optical approximation is valid only for a focused beam, or in other words for the Gaussian beam waist which is not subjected to diffraction beyond the zeroth order. We accomplish beam focusing using optical components with apertures of at least two inch (50.8 mm), this is 100 times larger than the $\lambda/2$ of 260 GHz radiation in order to avoid Fesnel diffraction or truncation of the Gaussian beam. All passive elements and the active manipulation of polarization and phase must meet the following criteria: $(i)$ minimal losses, $(ii)$ reproducibility of fine tuning and assembly, $(iii)$ flexibility in sources and their powers, and $(iv)$ ease of use. We discuss the selection, function and verification of these components in the following paragraphs.

*Passive quasioptical components.* The frequency tunable sub-THz radiation is provided by either a solid state source based on an yttrium-iron garnet oscillator[52] or a frequency tunable Gyrotron oscillator.[53] With a power loss of less than 5% per meter, this wave is transmitted through an overmoded waveguide (corrugated, stacked rings technology, Swissto12)[54] towards a position 8 cm before the mobile MP spectrometer board (Fig. 1). At this point, Gaussian beam propagation in free space takes place. Redirection and focusing of the quasioptical beam is achieved with gold-coated polished Cu mirrors. The

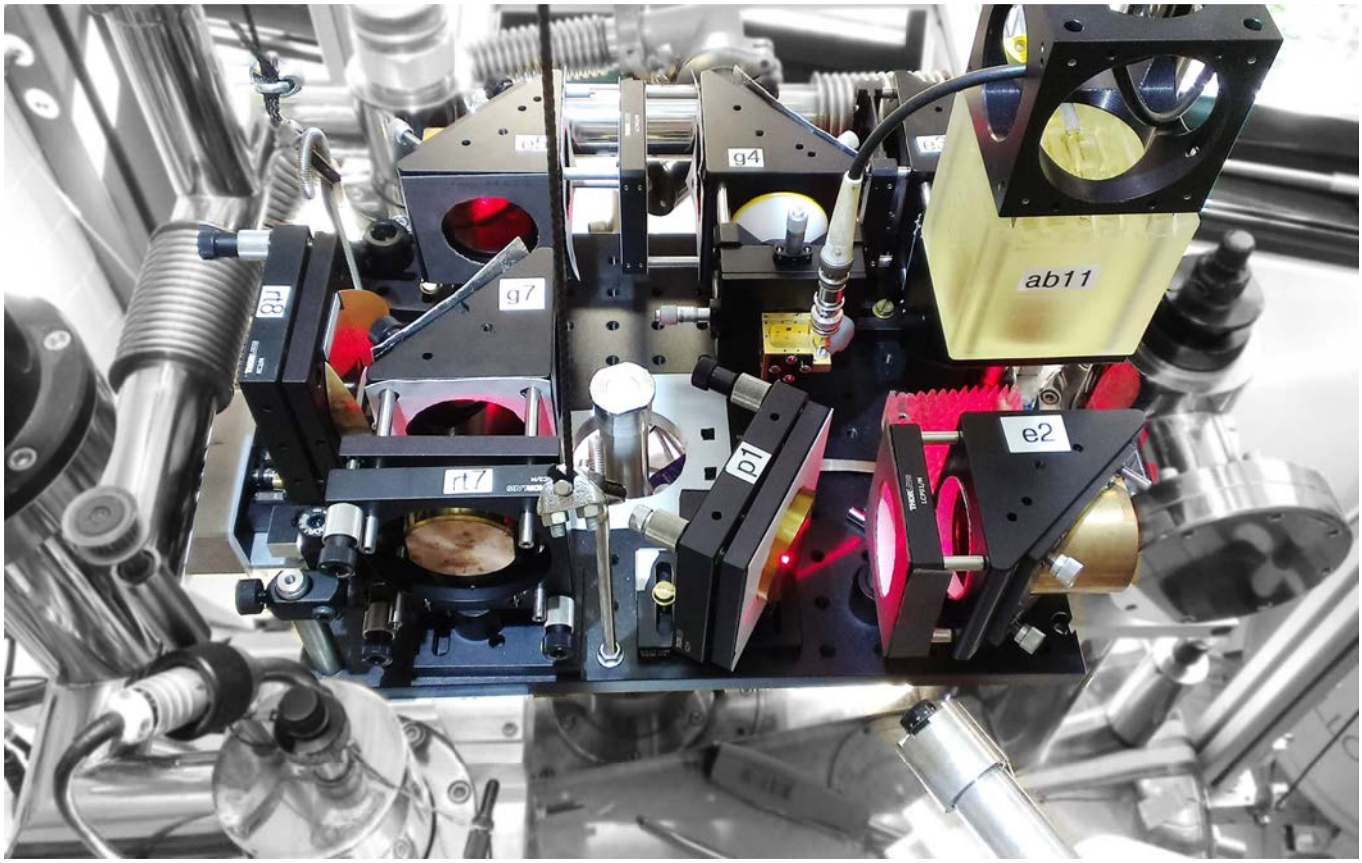


FIG. 3. Operating position of the mobile high-field quasioptical MP spectrometer on top of the Oxford 9.4 Tesla superconducting magnet with He cryostat. A collimated laser beam ($\lambda = 640$ nm, red) from the center of the corrugated source waveguide is used to align all passive components (e.g. mirrors and grids) in the orthogonal spectrometer design. To see the vertical corrugated waveguide (white), the central Miter bend was removed for the photograph.

first two mirrors are custom designed with a 90° off-axis parabolic surface so that the quasioptical beam is collimated and directed into the orthogonal system spanned by the edges of the board (Fig. 1). This allows us to use only $\pi/2$ reflections for which the foci can be controlled by elliptical mirrors. Two elliptical mirrors (curved in Fig. 1b) with focal length of 15 cm and 20 cm, repectively, keep the beam collimated. The collimated beam traverses two grids made of Au-coated W wire with 25 micron pitch,[55] which are at polar positions so as to transmit the incoming beam. When entering the Martin-Puplett interferometer (MPI), the sub-THz beam is polarized in a linear plane 45° off the vertical axis. The computer-controlled interferometer is described below, which controls the polarization and phase of the sub-THz radiation. A third 90° off-axis parabolic mirror directs the beam into the center of a vertical waveguide[54] which has the sample and modulation coil attached at its lower end. The sample holder comprises a focusing lens, a Helmholtz modulation coil and a plane reflection mirror which also serves to hold the sample (see Fig. 4 and the suppl. info.).

*Active polarization control.* Key to the function of a MPI is the control of the linear polarization. At the wire grid of the interferometer, the 45° off-axis linear polarized incident beam is split into the two interferometer arms equipped with roof top mirros of vertical mirror axes. The two beams have orthogonal polarizations. After reflection by the roof top mirrors, the polarization is rotated by 90° so that the two reflected beams pass through the central grid. While the fixed roof top mirror reflects the incoming beam with constant phase, the position of the mobile roof top mirror controlled on a sub-micrometer scale with a computer-driven step motor allows the selection of a phase by setting a boundary condition for the incoming coherent light. The phase retardation determines the axial ratio of elliptical polarization of the recombined beam after the grid: within a displacement of $|\lambda/2|$, the polarization changes from linear to elliptical and circular.

Figure 2a illustrates how a user can control the polarization which is sent towards the sample (red beam). A fine tuning of the interferometer pathway offers to the user a means for selecting the phase and the slope of the polarization change for detection with better SNR

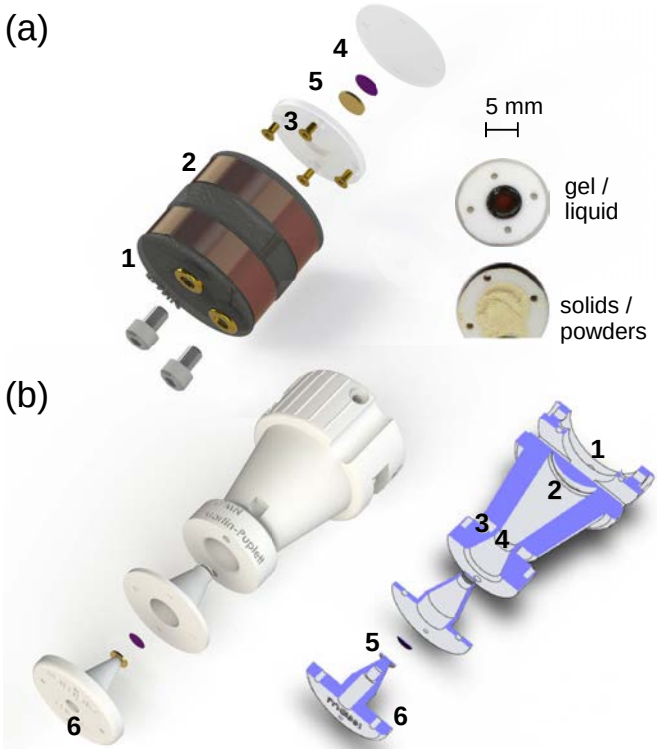


FIG. 4. Field modulation sample holders optimized for quasioptical ESR excitation and reflection. (a) Cryo-compatible oligomere resin (1) with Helmholtz coils (2), PTFE sample container (3), sample location (4) and Au reflector (5). (b) Room temperature sample holder with beam focusing and quick sample loading: threading for fixation to the waveguide (1), THz lens (2), solenoid coil (3), sample position (4), Au reflector (5) and sample position locking cone (6).

(green beam) — this is equivalent to phase selection using a frequency-locked detector known from conventional ESR. This phase and polarization control control can be actively accomplished by the computer-controlled interferometer arm. Its precision is 0.5 µm or $^1/_{2000}$ the wave length of 260 GHz radiation, and the adjustment within one $\lambda$ is accomplished in less than a second. While the phase is user-controlled before each ESR scan in this proof-of-principle study, developments are underway to use active computer control during acquisition, in order to account for wavelength phase changes in very broad scans or to compensate unwanted standing wave modes.

*ESR detection and standing wave management.* The signals returning from paramagnetic samples carry a rotated polarization which is the only component of the returning beam that is reflected by the wire grid to the detecting Schottky diode (Fig. 2a). However, a large fraction of the reflected beam does not carry information from the spins in resonance, as it was just reflected from a surface besides the sample position. These so-called standing waves (SW) can be orders of magnitude larger than the ESR signal and perturb the detection of smaller resonance signals. First, SW can be diminished by careful adjustment of the incoming beam to the centers of every aperture and by optimal collimation of the Gaussian beam (Fig. 3), in order to avoid scattering and Fresnel diffraction. Second, since mirror reflections cause no change in circularity — in contrast to the paramagnetic sample — reflected waves that contain no ESR information can be deflected by optical isolation. The optical isolator is the equivalent to a circulator in r.f. technology or to a rectifying diode in electronics: the millimeter waves pass only in one direction (Fig. 1a).[50] In addition to acting as a diode, the optical isolator in our MP spectrometer also directs reflected waves (i.e. having the wrong $\mathbf{k}$) into a 3D printed absorber and thus eliminates these SW modes from the optical path. Further details on optical isolation and the quasioptical beam propagation is compiled in the supplemental material.[56] Third, few SW modes with polarizations comparable to the sample signal can still travel into the detector and overlay the ESR. We can, nevertheless, identify these SW by a phase scan, which is recorded by a computer controlled linear sweep of the mobile roof top mirror in the MPI, spanning at least one wavelength. Herein, SW modes can be easily identified, since they are independent on field modulation and exhibit maxima at different phases than the ESR signal.

## MOBILITY AND VERSATILITY

In its standard operation, the MP spectrometer is installed on top of an Oxford 9.4 Tesla magnet with a variable temperature insert (Fig. 3). A key feature is its mobility: The compact quasi-optical bench can be lifted off and parked aside while other experiments are carried out with the magnet [56], thus seamlessly switching between high-field ESR and DNP-NMR experiments. Owing to its compactness and ruggedness, the MP spectrometer is also usable as a table-top device which can detect the magneto-optical properties of samples located in the central bore. It was used in this table-top-operation to characterize the polarization control of the interferometer, one part at a time.

Since the sub-THz source is located at the other end of the waveguide, it is easy to switch between two sources: Coherent radiation of (*i*) a solid state source with wide frequency range (245–280 GHz)[52] or (*ii*) a frequency tunable Gyrotron.[53, 56–58] Emission from the two sources was frequency-calibrated via quasioptical heterodyne detection (at 260 GHz, VDI) followed by an EIP Autohet frequency counter. The MP spectrometer is *broad band*, its only limitation is given by the Faraday rotators and the VDI Schottky diode detectors, whose performance drops beyond $\lambda_{260\,\mathrm{GHz}} \pm {}^{\lambda}/_{2}$, i.e. below 180 GHz or above 400 GHz.

If polarization analysis is not required, the quasiopti-

cal bridge can measure sample reflectivity, and the phase of reflected signals with 1 µm precision. Lastly, the MP spectrometer measures the power of the sub-THz source. It is advantageous to use the MP bridge for power measurements, because the fraction directed into the Schottky diode detector can be chosen by the active interferometer, and the VDI Schottky diode permits response linear in power from $10^{-9}$ V up to $10^{-2}$ V, where the latter corresponds to a maximal input power of $\sim 1$ W entering the quasioptical MP spectrometer at the end of source waveguide (Figs. 1–3).

## HIGH-FIELD QUASIOPTICAL ESR — PERFORMANCE TESTS

*DPPH — an organic ESR standard.* The organic chemical compound DPPH is a dark-blue stable free-radical, which provides one unpaired electron in the central nitrogen ion of every molecule, and is established to benchmark the position and intensity of ESR setups.[59] Recent studies tested this radical also as a polarizing agent for DNP-NMR,[60] and as quality indicator for southamerican coffee.[61] We conducted the high-field MP ESR at around 260 GHz with a broad band solid state source[52] using an output power of 80 mW.

Results of the DPPH electron spin resonance experiments are compiled in Fig. 5. In order to compare the benefit of the increased magnetic Zeeman splitting of high-field ESR ($B_0 = 9.28$ T) with conventional $X$ band ESR ($B_0 = 0.3$ T), panel (a) shows a field scan recorded at a frequency of 9.4 GHz while panel (b) depicts a high-field frequency scan of the same DPPH sample. Not only do we observe a sub-structure within the envelope of the well-known $X$ band scan, but the sensitivity is large enough to uncover more spectral features away from the main resonance. Five main peaks are hyperfine splittings (equidistant with 63 MHz) of the unpaired resonating electron $(\text{N–N})^\bullet$ with the two equivalent $^{14}$N nuclei of $I = 1$.[59, 60] We interprete the sub-structure (peak-to-peak distance 109 MHz) extending further apart from the dominant five peak structure as the hyperfine split contributions from $g$-tensor components different from $g_z$,[62, 63] which become resolvable thanks to the 29 times larger $B_0$ field compared to $X$ band ESR. Using the EasySpin simulation package,[64, 65] we could model the hyperfine split DPPH powder spectrum recorded at 9.28 T and determine three $g$-tensor components with individual hyperfine energies (Fig. 5c). Principal axes of $\mathbf{g}$ and $\mathbf{A}$ tensors were set parallel and $g$ anisotropy was found to be larger than in $X$ band ESR references of DPPH.[66, 67] Hereby, the simulated peak positions (blue) are convoluted with the interferometer amplitude response as a function of irradiation frequency (grey, in background) and with the natural width of the DPPH lines, yielding the spectrum (red). In summary, DPPH serves here as benchmark for the increased spectral frequency resolution and calibrates the MP spectrometer in the frequency domain.

*Sm-doped Ceria — catalyst and ionic conductor.* In a second step, we explore a functional oxide, $CeO_2$ micropowder, which is useful for various types of catalysis[18, 68] such as $CO_2$ reduction,[21, 25] Solid Oxide Fuel Cells[20, 69] and which even protects biologicals cells.[19] Ionic conductivity in Ceria requires oxygen vacancies or cationc sites with lower oxidation than $Ce^{4+}$ from the native lattice are required such as rare earth substitution with valency 3+. In order to test the ability of our MP

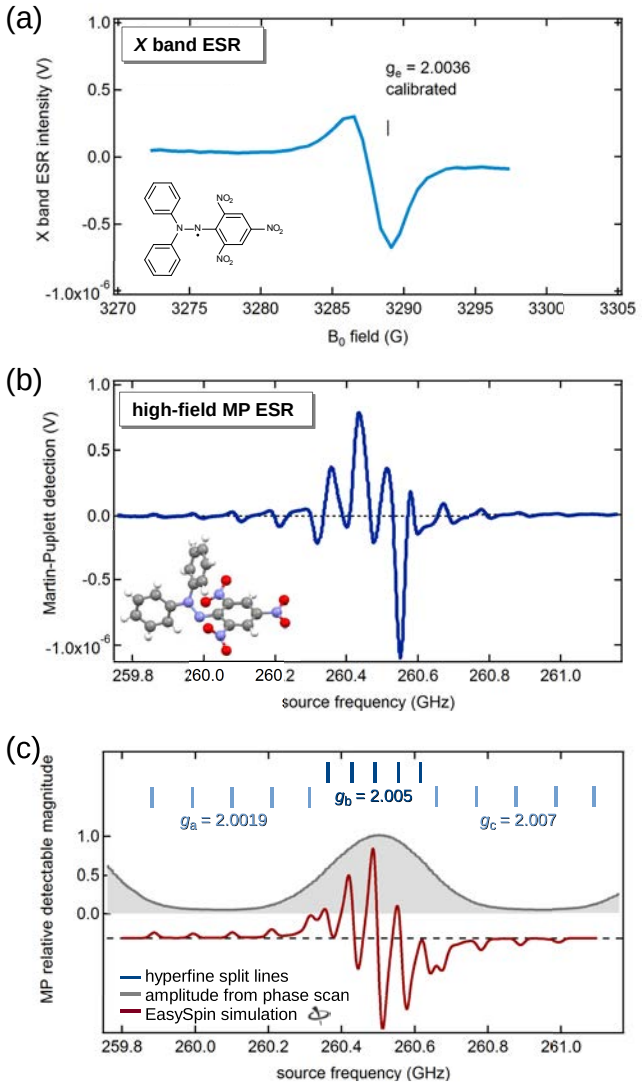


FIG. 5. ESR spectra of the stable organic radical 2,2-diphenyl-1-picrylhydrazyl (DPPH) solid micropowder taken at RT. $X$ band ESR (a) is compared with high-field ESR using the quasioptical MP spectrometer (b). Both measurements use the identical sample of solid DPPH with field modulation at RT, and 500 ms integration time. The hyperfine split peaks are identified and modeled in (c).

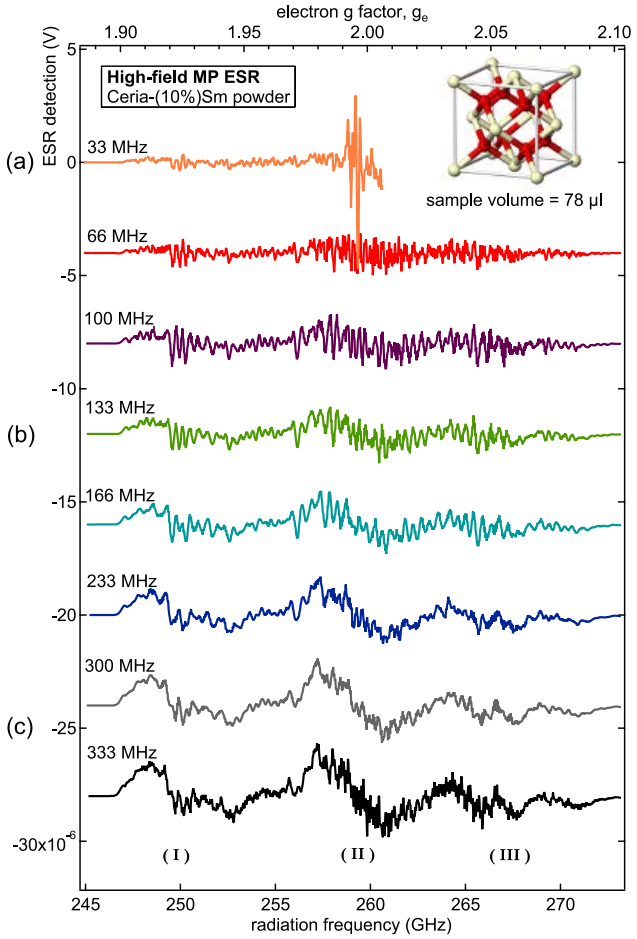


FIG. 6. Frequency modulation high-field ESR spectra of Sm(10%)-doped Ceria micropowder, taken at RT using 500 ms integration time. Region (a) uses smallest frequency modulation of the quasioptical irradiation, and regions (b) to (c) show the spectra with increasing and maximal freuqncy modulation width. Three groups of ESR peaks are indicated in roman numbers.

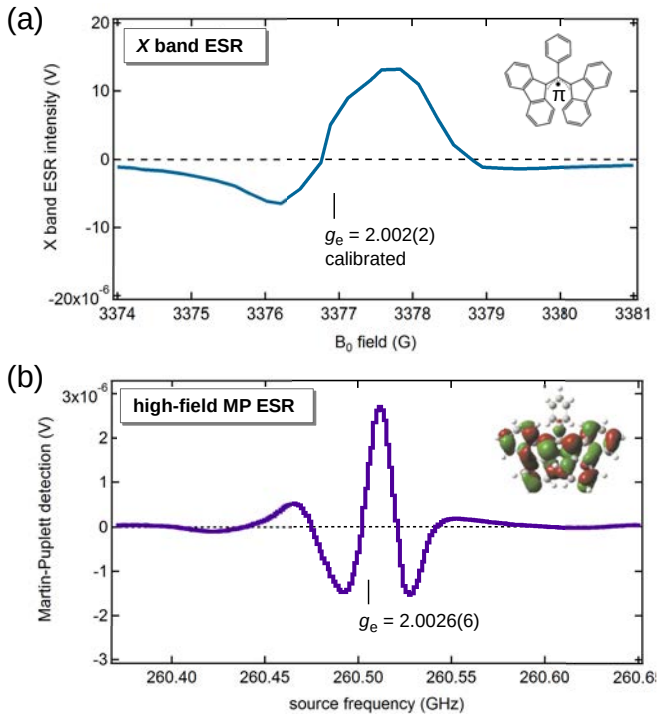


FIG. 7. $X$ band (a) and high-field 260 GHz ESR spectra (b) of the same stable organic radical 1,3-bisdiphenylene-2-phenylallyl in polystyrene matrix (BDPA). Measurements are taken at RT using $B_0$ field modulation, and 500 ms integration time.

spectrometer to detect the presence of various radicals with $g$ near 2, we investigated Samarium-doped Ceria powder ($Sm_\alpha\, Ce_{1-\alpha}\, O_2$, $\alpha = 10\%$).

Figure 6 compiles the high-field quasioptical ESR study of Sm:$CeO_2$ at room temperature. In contrast to the sharp electronic spin resonance of e.g. DPPH ($2p$ electron), the resonance is very broad, it originates from $Sm^{3+}$. A characteristic of the unpaired $4f$ electron is the broadly distributed and feature rich ESR spectrum (Fig. 6). Only at the smallest modulation width ($\Delta f_{h\nu} \leqslant 33\,\mathrm{MHz}$), a narrow resonance is obervable at $g = 1.995$, which can be ascribed to oxygen vacancies in the Ceria lattice.[22, 23, 70] The weaker and broad resonances from the $4f$ unpaired electrons are observable only if frequency modulation is used with the maximum available breadth of frequency modulation ($\Delta f_{h\nu} \overset{\max}{\dashrightarrow} 350\,\mathrm{MHz}$).[52] The distribution of the spectral features might be explained by strong spin-orbit coupling in $4f$ electrons. We identify three major regions: a central peak at $f = 259.5\,\mathrm{GHz}$ and two regions comprising several peaks of less magnitude from 245–252 GHz and 265–268 GHz. This corresponds to $g$-factors of the $Sm^{3+}$ sites ranging from 1.9 to 2.06, and indeed literature reports broadly distributed theoretical expectations of $g$-factors from Sm ions.[26, 70, 71]. Further work is ongoing to characterize the radicals in this functional oxide.

In summary, the study of Sm-doped Ceria powder successfully demostrates the flexibility of high-field quasioptical MP detection using *frequency modulation* in order to detect weak and very broad electron spin resonances as well as narrow $O^\bullet$ lines.

*BDPA — narrow high-field ESR standard and DNP-NMR.* To test our setup further, we examined the radical BDPA, in view of its interest in DNP-NMR.[60, 72, 73] The stable free radical BDPA has an unpaired carbon $\pi$ electron that delocalizes over the radical backbone in the singly occupied molecular orbital (inset in Fig. 7a). The high-field quasioptical ESR study (Fig. 7b) shows the BDPA signal to be narrow (HWFM $\approx 15\,\mathrm{MHz}$) and of moderate intensity compared with the prominent signal of DPPH (comparable spins in Fig. 5). Comparing $X$ band ESR (a) with high-field 260 GHz ESR (b) of

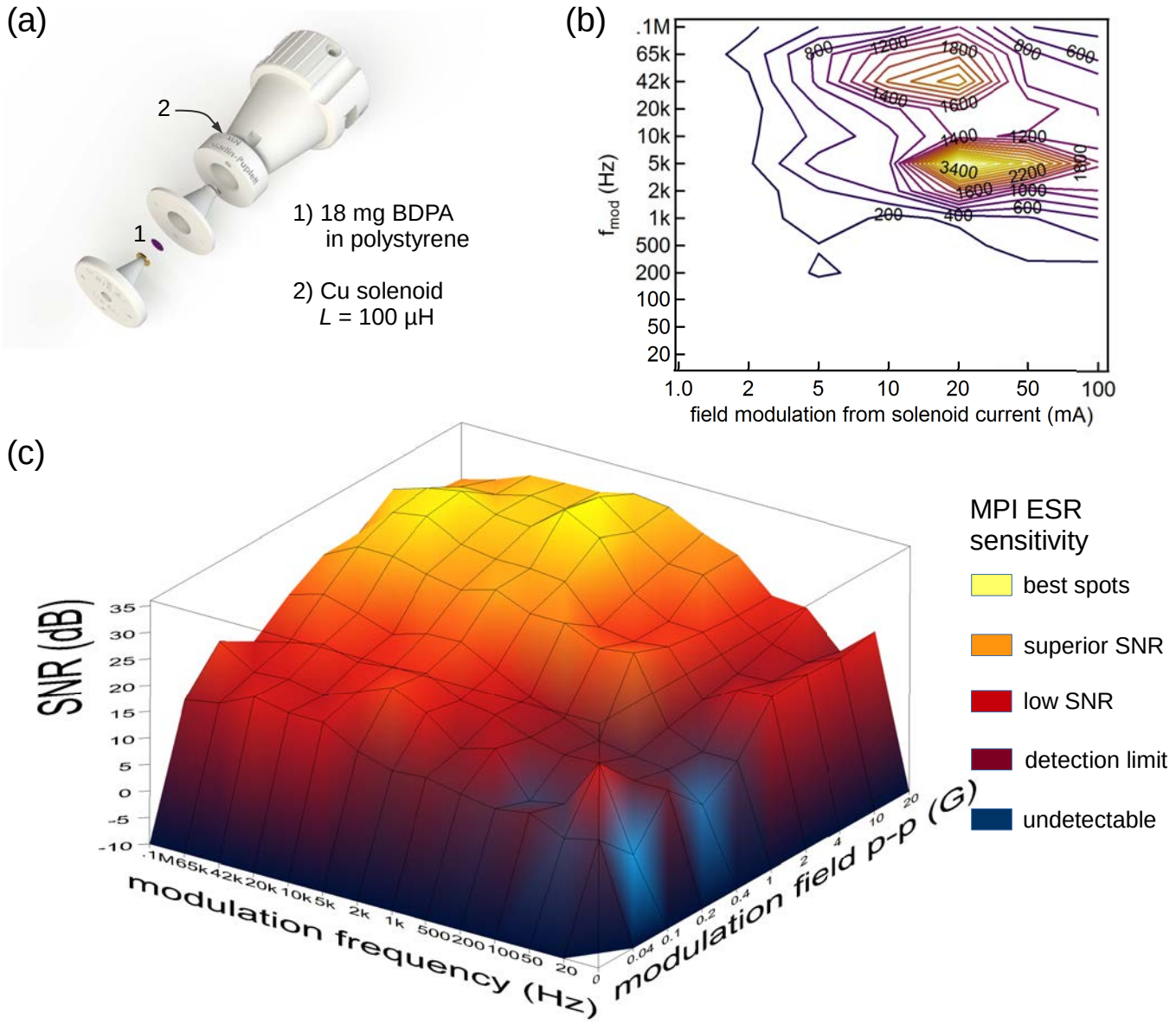


FIG. 8. Quasioptical MP ESR spectrometry with BDPA loaded into the focusing quick load sample holder (a) and 70 mW coherent sub-THz irradiation. The figure of merit displays the possible regions of the quasioptical ESR detection as a function of the field modulation (b). The full analysis of the detectable SNR for the $B_0$ field modulation is mapped vs frequency and modulation amplitude in (c).

the same BDPA, we find and increase of spectral resolution of a factor 10, this is however limited by the natural width of the BDPA resonace. Deconvolution reveals two spectral features separated by 44 MHz, which agrees well with $g$-tensor anisotropy of the BDPA molecule.[74]

In summary, the stable radical BDPA showed two well-distinguishable sharp spectral peaks in the high-field ESR at RT. Such exact knowledge of the electronic resonance frequency is of immediate use for DNP-NMR, since dynamic nuclear polarization through Overhauser or Solid effects requires narrow line radicals and a very precise knowledge of their $g$-factors.[60, 74]

Since the peak characteristics of BDPA exhibit one single feature and narrow peak width, this system is perfectly suitable for testing the achievable spin sensitivity of the quasioptical MP ESR spectrometer.

*Optimal operation parameters using quasioptical focusing and field modulation.* BDPA in polystyrene matrix is used to explore the operating conditions of the new high-field quasioptical MP ESR spectrometer equipped with the 3D laser-melted beam focusing sample stage (Fig. 4b). Here we search for the optimum conditions for the frequency and the amplitude of the field modulation using a low-inductance solenoid, which is integrated

with the focusing sample stage.

Figure 8 shows the operation range in which high-field ESR detection is possible: blue areas provide thermal noise, whereas dark red regions ($f^{\mathrm{mod}} \geqslant 20\,\mathrm{Hz}$; $B_0^{\mathrm{mod}} \geqslant 0.04\,\mathrm{G}$) render ESR detection possible with $1 \leqslant \mathrm{SNR} \leqslant 10$. Except for a clear valley of SNR at modulation frequencies of 50–100 Hz, the system has a very broad operability using the quasioptical sample stage thanks to a low-inductance modulation coil (Fig. 8a).

We identified two *sensitivity* maxima (Fig. 8b): First, at modulation amplitudes of 4–10 G and frequencies ∼5 kHz, a maximal SNR of 3600 can be reached. Second, a modulation speed to 42 kHz leads to a second maximum of SNR ≈ 2400. Beyond this speed, inductive reactance is limiting field modulation, and the SNR does not increase further. A performance analysis of the field modulation is given in the supplemental information.[56] Since the sample contained 18 mg of BDPA, by extrapolating the SNR from its optimum value to a value of one we find that our MP spectrometer can in principle detect a number of spins of

$$N_{\mathrm{min}}^{\mathrm{spins}} = (1.0 \pm 0.5) \times 10^{14}. \qquad (2)$$

We recall that our setup uses direct reflection and does not use any resonator.

The highest *spectral resolution* is achieved if $B_0^{\mathrm{mod}} \leqslant 0.04\,\mathrm{G}$ (FWFM ≈ 15 MHz) at which the natural width of the BDPA spectral feature is asymptotically reached.[56]

## SUMMARY AND OUTLOOK

We demonstrated the successful implementation of a fully functional high-field quasioptical ESR spectrometer with selectable sub-THz sources.

Key features which contribute to a better signal-to-noise ratio and sensitivity comprise the actively controlled MP interferometer, the passive optical isolation against standing wave modes, and the optically focused free space wave propagation within the ESR spectrometer. Care was taken to design the ESR spectrometer so that it is mechanically stable and reproducible by using microprecision standard parts.[49] The spectrometer features mobility by a crane system and versatility by the use as table-top system (see supporting information and video[56]).

First high-field quasioptical ESR results include the standard radical DPPH (resonance from $(\mathrm{N–N})^{\bullet}$), Sm-doped Ceria powder (resonance from $4f^{\bullet}$), and BDPA (resonance from $\mathrm{C}^{\bullet}$), all of which reveal spectral substructures invisible at conventional $X$ band ESR. By combing a quasioptically focusing sample stage with $B$ field modulation at high frequencies we reached SNRs up to 3600 using a BDPA sample with $\sim 10^{18}$ spins.

From the BDPA studies, we conclude that a detection sensitivity of at least $10^{14}$ spins is feasible using the $P = 80\,\mathrm{mW}$ solid state source, which is encouraging for obtaining paramagnetic resonance signals of oxide surfaces. Thanks to the design of high radiation power acceptance (several watts), the presented quasioptical ESR spectrometer will ultimately permit the in-line use with the DNP-NMR experiment driven by frequency tunable Gyrotron radiation.

CC acknowledges helpful discussion with Dongyoung Yoon and Swissto12.[75] We acknowledge excellent support in engineering and construction by Gilles Grandjean and Adrien Grisendi. PFS was supported by EPFL-LPMN. VDI instrumentation was financed through Swissto12 by the CTI grant No. 15617.1 PFNM-NM. The Gyrotron oscillator was funded by R'Equip (No. 206021-121303/1) and Sinergia grants (No. CRSI20-122708/1, No. 200020-120503/1) of the SNSF.

* christian.caspers@epfl.ch; http://lpmn.epfl.ch

[1] E. Zavoisky, J Phys (USSR) **9**, 245 (1945).
[2] C. Di Valentin, G. Pacchioni, A. Selloni, S. Livraghi, and E. Giamello, The Journal of Physical Chemistry B **109**, 11414 (2005), pMID: 16852395, http://dx.doi.org/10.1021/jp051756t.
[3] C. Caspers, M. Müller, A. X. Gray, A. M. Kaiser, A. Gloskovskii, C. S. Fadley, W. Drube, and C. M. Schneider, physica status solidi (RRL) Rapid Research Letters **5**, 441 (2011).
[4] A. M. Kolpak and S. Ismail-Beigi, Phys. Rev. B **85**, 195318 (2012).
[5] R. Oja, M. Tyunina, L. Yao, T. Pinomaa, T. Kocourek, A. Dejneka, O. Stupakov, M. Jelinek, V. Trepakov, S. van Dijken, and R. M. Nieminen, Phys. Rev. Lett. **109**, 127207 (2012).
[6] H. Y. Hwang, Y. Iwasa, M. Kawasaki, B. Keimer, N. Nagaosa, and Y. Tokura, Nat Mater **11**, 103 (2012).
[7] J.-S. Lee, in *Bulletin of the American Physical Society*, Vol. 60 (2015) pp. MAR15–2014–020113, MAR15-2014-020113.
[8] I. P. Bykov, M. D. Glinchuk, V. V. Laguta, A. M. Slipenyuk, S. M. Korniyenko, L. Soukup, L. Jastrabik, and A. Dejneka, Ferroelectrics **239**, 349 (2000), http://dx.doi.org/10.1080/00150190008213341.
[9] S. Gallego, J. I. Beltran, J. Cerda, and M. C. Munoz, Journal of Physics: Condensed Matter **17**, L451 (2005).
[10] C. Gionco, E. Giamello, L. Mino, and M. C. Paganini, Phys. Chem. Chem. Phys. **16**, 21438 (2014).
[11] J. Rocker, D. Cornu, E. Kieseritzky, A. Seiler, O. Bondarchuk, W. Hänsel-Ziegler, T. Risse, and H.-J. Freund, Review of Scientific Instruments **85**, 083903 (2014).
[12] L.-B. Xiong, J.-L. Li, B. Yang, and Y. Yu, Journal of Nanomaterials **2012**, 13 (2012).
[13] N. C. Plumb, M. Salluzzo, E. Razzoli, M. Månsson, M. Falub, J. Krempasky, C. E. Matt, J. Chang, M. Schulte, J. Braun, H. Ebert, J. Minár, B. Delley, K.-J. Zhou, T. Schmitt, M. Shi, J. Mesot, L. Patthey, and M. Radović, Phys. Rev. Lett. **113**, 086801 (2014).
[14] A. F. Santander-Syro, F. Fortuna, C. Bareille, T. C. Roedel, M.del, G. Landolt, N. C. Plumb, J. H. Dil, and M. Radovic, Nat Mater **13**, 1085 (2014).
[15] W. Rice, P. Ambwani, M. Bombeck, J. D. Thompson,

G. Haugstad, C. Leighton, and S. Crooker, Nat Mater **13**, 481 (2014).
[16] S. Crooker, in *Bulletin of the American Physical Society*, Vol. 60 (2015) pp. MAR15–2014–020056, MAR15-2014-020056.
[17] M. Che, J. F. J. Kibblewhite, A. J. Tench, M. Dufaux, and C. Naccache, J. Chem. Soc., Faraday Trans. 1 **69**, 857 (1973).
[18] S. Ackermann, L. Sauvin, R. Castiglioni, J. L. M. Rupp, J. R. Scheffe, and A. Steinfeld, The Journal of Physical Chemistry C **119**, 16452 (2015), http://dx.doi.org/10.1021/acs.jpcc.5b03464.
[19] F. Caputo, M. De Nicola, A. Sienkiewicz, A. Giovanetti, I. Bejarano, S. Licoccia, E. Traversa, and L. Ghibelli, Nanoscale **7**, 15643 (2015).
[20] V. Kharton, F. Figueiredo, L. Navarro, E. Naumovich, A. Kovalevsky, A. Yaremchenko, A. Viskup, A. Carneiro, F. Marques, and J. Frade, Journal of Materials Science **36**, 1105 (2001).
[21] A. Aboukais, E. A. Zhilinskaya, J.-F. Lamonier, and I. N. Filimonov, Colloids and Surfaces A: Physicochemical and Engineering Aspects **260**, 199 (2005).
[22] P. Lakshmanan, F. Averseng, N. Bion, L. Delannoy, J.-M. Tatibout, and C. Louis, Gold Bulletin **46**, 233 (2013).
[23] M. D. Hernández-Alonso, A. B. Hungría, A. Martínez-Arias, M. Fernández-García, J. M. Coronado, J. C. Conesa, and J. Soria, Applied Catalysis B: Environmental **50**, 167 (2004).
[24] H. A. Al-Madfa, M. M. Khader, and M. A. Morris, International Journal of Chemical Kinetics **36**, 293 (2004).
[25] N. Kumari, N. Sinha, M. Haider, and S. Basu, Electrochimica Acta **177**, 21 (2015).
[26] S. Vahedi, G. Okada, C. Koughia, R. Sammynaiken, A. Edgar, and S. Kasap, Opt. Mater. Express **4**, 1244 (2014).
[27] D. M. Murphy and M. Chiesa, in *Electron Paramagnetic Resonance*, Vol. 21 (The Royal Society of Chemistry, 2008) pp. 105–130.
[28] Y. S. Lebedev, *High-Frequency Continuous-Wave Electron Spin Resonance* (Wiley, NY, 1990) pp. 365–404.
[29] W. B. Lynch, K. A. Earle, and J. H. Freed, Review of Scientific Instruments **59**, 1345 (1988).
[30] G. Eaton and S. Eaton, Applied Magnetic Resonance **16**, 161 (1999).
[31] J. H. Freed, Annual Review of Physical Chemistry **51**, 655 (2000), pMID: 11031296, http://dx.doi.org/10.1146/annurev.physchem.51.1.655.
[32] M. Bennati and T. F. Prisner, Reports on Progress in Physics **68**, 411 (2005).
[33] O. Grinberg and L. Berliner, *Very High Frequency (VHF) ESR/EPR*, Biological Magnetic Resonance (Springer US, 2013).
[34] K. A. Earle, J. H. Freed, and D. E. Budil (Academic Press, 1996) pp. 253 – 323.
[35] K. A. Earle, D. S. Tipikin, and J. H. Freed, Review of Scientific Instruments **67**, 2502 (1996).
[36] D. Schmalbein, G. Maresch, A. Kamlowski, and P. Hfer, Applied Magnetic Resonance **16**, 185 (1999).
[37] B. Náfrádi, R. Gaál, A. Sienkiewicz, T. Fehér, and L. Forró, Journal of Magnetic Resonance **195**, 206 (2008).
[38] A. Savitsky and K. Möbius, Photosynthesis Research **102**, 311 (2009).
[39] K. L. Nagy, D. Quintavalle, T. Fehér, and A. Jánossy, Applied Magnetic Resonance **40**, 47 (2011).
[40] J. Yan, L. Barnett, C. Domier, and N. C. Luhmann, Proc. SPIE **8496**, 84960D (2012).
[41] A. Hassan, A. Maniero, H. van Tol, C. Saylor, and L.-C. Brunel, Applied Magnetic Resonance **16**, 299 (1999).
[42] S. Takahashi, D. G. Allen, J. Seifter, G. Ramian, M. S. Sherwin, L.-C. Brunel, and J. van Tol, Infrared Physics & Technology **51**, 426 (2008), 4th International Workshop on Infrared Microscopy and Spectroscopy with Accelerator-Based Sources.
[43] S. Takahashi, L.-C. Brunel, D. T. Edwards, J. van Tol, G. Ramian, S. Han, and M. S. Sherwin, Nature **489**, 409 (2012).
[44] S. A. Zvyagin, M. Ozerov, E. Cizmár, D. Kamenskyi, S. Zherlitsyn, T. Herrmannsdörfer, J. Wosnitza, R. Wünsch, and W. Seidel, Review of Scientific Instruments **80**, 073102 (2009).
[45] J. van Tol, L.-C. Brunel, and R. J. Wylde, Review of Scientific Instruments **76**, 074101 (2005), 10.1063/1.1942533.
[46] I. Gromov and P. Höfer, in *Euromar 2013* (EPR Division, Bruker Biospin GmbH, 76287 Rheinstetten, Germany).
[47] B. D. Armstrong, D. T. Edwards, R. J. Wylde, S. A. Walker, and S. Han, Phys. Chem. Chem. Phys. **12**, 5920 (2010).
[48] D. Martin and E. Puplett, Infrared Physics **10**, 105 (1970).
[49] Thorlabs inc., "60 mm cage system optic mounts," (2015), copyright 1999-2015 Thorlabs, Inc.
[50] D. Martin, R. Wylde, and R. Wylde, Microwave Theory and Techniques, IEEE Transactions on **57**, 99 (2009).
[51] D. T. Chuss, S. H. Moseley, G. Novak, and E. J. Wollack, Proc. SPIE **5492**, 1487 (2004).
[52] Virginia Diodes inc., "VAdiodes.com," (2015), Sub-THz transmitter, part No Tx-237.
[53] S. Alberti, J.-P. Ansermet, K. A. Avramides, F. Braunmueller, P. Cuanillon, J. Dubray, D. Fasel, J.-P. Hogge, A. Macor, E. de Rijk, M. da Silva, M. Q. Tran, T. M. Tran, and Q. Vuillemin, Physics of Plasmas (1994-present) **19**, 123102 (2012).
[54] E. de Rijk, A. Macor, J.-P. Hogge, S. Alberti, and J.-P. Ansermet, Review of Scientific Instruments **82**, 066102 (2011).
[55] P. Ade, A. Costley, C. Cunningham, C. Mok, G. Neill, and T. Parker, Infrared Physics **19**, 599 (1979).
[56] C. Caspers, "Martin-Puplett ESR spectrometer mobility and versatility," (2015), supplemental multimedia movie.
[57] S. Alberti, F. Braunmueller, T. M. Tran, J. Genoud, J.-P. Hogge, M. Q. Tran, and J.-P. Ansermet, Phys. Rev. Lett. **111**, 205101 (2013).
[58] J.-P. Hogge, F. Braunmueller, S. Alberti, J. Genoud, T. Tran, Q. Vuillemin, M. Tran, J.-P. Ansermet, P. Cuanillon, A. Macor, E. de Rijk, and P. Saraiva, in *Infrared, Millimeter, and Terahertz Waves (IRMMW-THz), 2013 38th International Conference on* (2013).
[59] J. Krzystek, A. Sienkiewicz, L. Pardi, and L. Brunel, Journal of Magnetic Resonance **125**, 207 (1997).
[60] L. Lumata, M. Merritt, C. Khemtong, S. J. Ratnakar, J. van Tol, L. Yu, L. Song, and Z. Kovacs, RSC Adv. **2**, 12812 (2012).
[61] J. H. O. Barbosa, J. A. G. Luna, A. M. O. Kinoshita, and O. Baffa Filho, Ciêencia e Agrotecnologia **37**, 495 (2013).
[62] S. Kolaczkowski, J. Cardin, and D. Budil, Applied Mag-

netic Resonance **16**, 293 (1999).
[63] A. Abragam, "The principles of nuclear magnetism," (Clarendon Press, 1983) Chap. VI — Electron-Nucleus interactions, p. 191ff.
[64] S. Stoll and A. Schweiger, Journal of Magnetic Resonance **178**, 42 (2006).
[65] S. Stoll, in *Electron Paramagnetic Resonance Investigations of Biological Systems by Using Spin Labels, Spin Probes, and Intrinsic Metal Ions, Part A*, Methods in Enzymology, Vol. 563, edited by P. Z. Qin and K. Warncke (Academic Press, 2015) pp. 121 – 142.
[66] R. W. Holmberg, "A paramagnetic resonance study of hyperfine interactions in single-crystals containing a,$\alpha$-diphenyl-$\beta$picrylhydrazil," (1961).
[67] H. D. Wijn and J. Henning, Physica **28**, 592 (1962).
[68] R. J. Gorte, AIChE Journal **56**, 1126 (2010).
[69] S.-F. Wang, C.-T. Yeh, Y.-R. Wang, and Y.-C. Wu, Journal of Materials Research and Technology **2**, 141 (2013).
[70] A. Sienkiewicz, "On high-field ESR spectra of Sm-$CeO_2$," priv. comm. (2015).
[71] D. Hui-Ning, Z. Wen-Chen, W. Shao-Yi, and T. Sheng, Spectrochimica Acta Part A: Molecular and Biomolecular Spectroscopy **60**, 489 (2004).
[72] L. Lumata, S. J. Ratnakar, A. Jindal, M. Merritt, A. Comment, C. Malloy, A. D. Sherry, and Z. Kovacs, Chemistry A European Journal **17**, 10825 (2011).
[73] T. V. Can, M. A. Caporini, F. Mentink-Vigier, B. Corzilius, J. J. Walish, M. Rosay, W. E. Maas, M. Baldus, S. Vega, T. M. Swager, and R. G. Griffin, The Journal of Chemical Physics **141**, 064202 (2014).
[74] L. Becerra, G. Gerfen, B. Bellew, J. Bryant, D. Hall, S. Inati, R. Weber, S. Un, T. Prisner, A. McDermott, K. Fishbein, K. Kreischer, R. Temkin, D. Singel, and R. Griffin, Journal of Magnetic Resonance, Series A **117**, 28 (1995).
[75] Swissto12 SA, "Swissto12.ch," (2015), terahertz applications.